RSC Advances

A Stereoregular Macrocyclic Oligomeric Silsesquioxane Bearing Epoxide Groups: Synthesis and Its Nanocomposites with Polybenzoxazine

Journal:	*RSC Advances*
Manuscript ID:	RA-ART-07-2015-012843.R2
Article Type:	Paper
Date Submitted by the Author:	03-Sep-2015
Complete List of Authors:	Wei, Kun; Shanghai Jiao Tong Univeristy, Department of Polymer Science and Engineering Liu, Ning; Shanghai Jiao Tong Univeristy, Department of Polymer Science and Engineering Li, Lei; Shanghai Jiao Tong University, Department of Polymer Science and Engineering Zheng, Sixun; Shanghai Jiao Tong Univeristy, Department of Polymer Science and Engineering

Graphical Abstract

A Stereoregular Macrocyclic Oligomeric Silsesquioxane Bearing Epoxide Groups: Synthesis and Its Nanocomposites with Polybenzoxazine

Kun Wei, Ning Liu, Lei Li and Sixun Zheng*

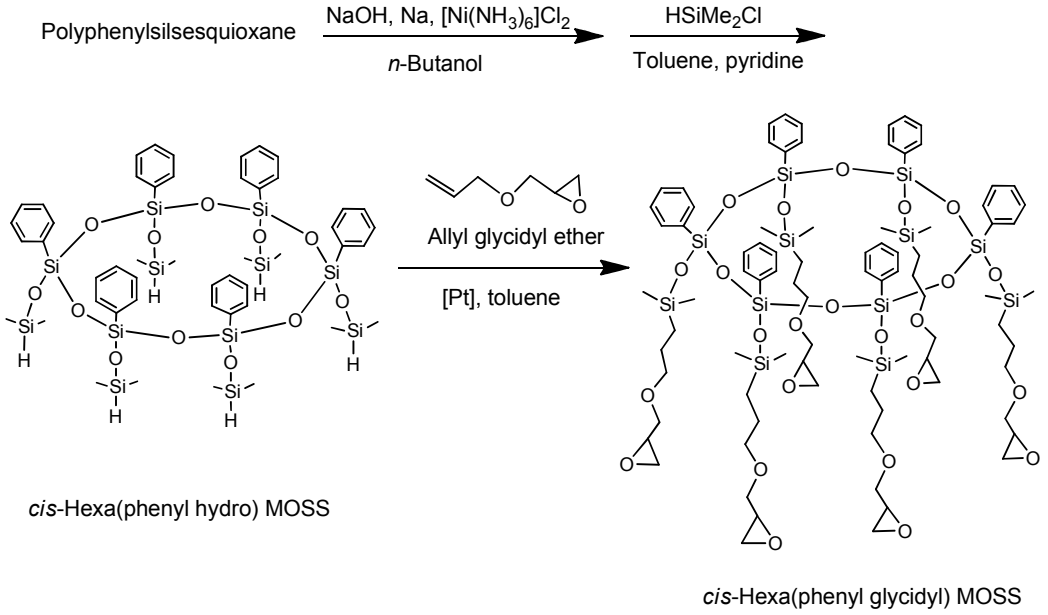

cis-Hexa(phenyl glycidyl) MOSS, a novel macrocyclic oligomeric silsesquioxane (MOSS) was synthesized and incorporated into polybenzoxazine to obtain the organic-inorganic nanocomposites.

A Stereoregular Macrocyclic Oligomeric Silsesquioxane Bearing Epoxide Groups: Synthesis and Its Nanocomposites with Polybenzoxazine

Kun Wei, Ning Liu, Lei Li and Sixun Zheng*

Department of Polymer Science and Engineering and the State Key Laboratory of Metal Matrix Composites, Shanghai Jiao Tong University, Shanghai 200240, P. R. China

* To whom correspondence should be addressed. Email: *szheng@sjtu.edu.cn (S. Zheng)*; Tel: 86-21-54743278; Fax: 86-21-54741297.

ABSTRACT

In this contribution, we reported the synthesis of *cis*-hexa[(phenyl)(dimethylsiloxypropylglycidylether)cyclohexasiloxane, a novel macrocyclic oligomeric silsesquioxane (MOSS) *via* the combination of silylation and hydrosilylation reactions. This stereoregular MOSS macromer bearing epoxide groups was then incorporated into polybenzoxazine (PBZ) thermoset and the organic-inorganic nanocomposites were successfully obtained as evidenced by scanning electron microscopy (SEM) and transmission electron microscopy (TEM). Dynamic mechanical thermal analysis (DMTA) showed that the organic-inorganic nanocomposites displayed the enhanced glass transition temperatures (T_g's) compared to plain PBZ. Thermogravimetric analysis (TGA) indicates that the organic-inorganic PBZ nanocomposites possessed the improved thermal stability. The improved thermomechanical properties are attributable to the nanoreinforcement of the stereoregular macrocyclic silsesquioxanes on PBZ matrix as well as the additional crosslinking between PBZ and the MOSS macromer. The results of static contact angle measurement showed that the surface hydrophobicity of the organic-inorganic nanocomposites was significantly improved compared to plain PBZ thermoset.

(**Keywords:** macrocyclic oligomeric silsesquioxane; polybenzoxazine; nanocomposites; thermomechanical properties)

INTRODUCTUON

Incorporating well-defined inorganic or organometallic blocks into organic polymers to afford organic-inorganic nanocomposites is one of the most important approaches to develop new materials. Stereoregular oligomeric silsesquioxanes have recently emerged as a class of new building blocks for the inorganic-organic hybrids [1-9]. Of them, polyhedral oligomeric silsesquioxanes (POSS) are a class of interesting stereoregular oligomeric clusters, each of which is composed of a cage-like Si-O framework with a nanometer size and organic groups covalently bonded to each Si atom [2-5]. In the past years, POSS and POSS-containing nanocomposites have become the focus of many studies since this class of organic-inorganic hybrids can display excellent comprehensive properties through the synergism of organic and inorganic components [7-9]. The utilization of stereoregular oligomeric silsesquioxanes as the building blocks to access the organic-inorganic nanocomposites is on the basis of their elemental and structural features: i) the organic-inorganic assemblies with reactive functional groups, which display the affinity with organic and inorganic materials and ii) the rigid stereoregular nanostructures, which can reinforce matrixes of organic polymers on the segmental scale.

Polyhedral oligoalkylmetallasiloxanes are a class of novel organometallic compounds, which consist of stereoregular alkylsiloxane macrocycles coordinated to alkaline and/or transition metals (*e.g.*, Mn, Co, Ni, Cu and trivalent lanthanide metals) [10-15]. In the early 1990s, Shchegolikhina *et al.* [14,16,17] first reported several examples of these compounds with a three-step reaction methodology with high yields. More importantly, these metallasiloxane coordinates can conveniently be derived into macrocyclic oligomeric silsesquioxanes (MOSS) *via* silylation reaction with satisfactory yields (Scheme 1). In limited literature [10-17], macrocyclic oligomeric silsesquioxanes have been prepared for the purpose of the structural analysis of their precursor of metallasiloxane coordinates. Due to their elemental and nanostructural features, functionalized MOSS macromers should be able to use as a class of new building blocks for the organic-inorganic hybrids as functionalized POSS macromers. In the previous works, we have explored such utilization [18-23]. For instance, we ever synthesized two polymerizable MOSS macromers bearing both vinyl groups and Si-H bonds, which can undergo the self-polymerization of hydrosilylation to afford highly porous polysilsesquioxane networks [18]. More recently, several 24-membered

macrocycles of silsesquioxanes bearing vinyl, hydroxyl groups have been used as the building blocks to obtain the macrocyclic molecular brushes bearing homopolymer or block copolymer side chains [21,22]. However, such a study remains largely unexplored. To the best of our knowledge, there has been no precedent report on the utilization of MOSS macromers as the nanoreinforcement agents of thermosetting polymers.

Polybenzoxazines (PBZ) are a class of novel phenolic resins, which possess excellent thermal, mechanical properties and electrical properties [24]. PBZ thermosets can be obtained *via* thermally activated ring-opening polymerization of benzoxazine monomers (BZ) and no hardeners are necessarily involved with the curing process. PBZ are a promising alternative to some traditional thermosets such as epoxy, phenolic and bismaleimide resins [25-38]. However, PBZ thermosets inherently possessed some drawbacks in properties. For instance, the mechanical strength of PBZ thermosets in the rubbery state is quite poor since the crosslinking densities of the thermosets are relatively low compared to other thermosetting polymers [39]. In addition, the glass transition temperature (T_g) of PBZ is only *c.a.* 150 ^oC, which is not sufficiently high for the application as the matrix of some high performance composites. The potential application of PBZ motivates to improve the thermomechanical properties of the thermoset. In the past years, there have been a great number of reports on the modification of PBZ thermoset by the use of organosilicon compounds such as polydimethylsiloxane elastomer and polyhedral oligomeric silsesquioxanes (POSS) [40]. To the best of our knowledge, there has been no precedent report on the investigation of the PBZ nanocomposites containing macrocyclic oligomeric silsesquioxanes (MOSS).

In this work, we explored to improve the thermomechanical properties of PBZ by incorporating a multifunctional stereoregular macrocyclic oligomeric silsesquioxane (MOSS). Toward this end, we first explored to synthesize *cis*-hexa[(phenyl)(demethylsiloxypropylglycidylether)cyclohexasiloxane [denoted *cis*-hexa(phenyl glycidyl) MOSS], a novel macrocyclic oligomeric silsesquioxane *via* the combination of silylation and hydrosilylation reactions. Thereafter, this functional MOSS macromer was incorporated into PBZ to obtain the organic-inorganic nanocomposites. The morphology of the organic-inorganic nanocomposites was investigated by means of scanning electron calorimetry (SEM) and transmission

electron microscopy (TEM); the thermomechanical properties were addressed on the basis of dynamic mechanical thermal analysis (DMTA) and thermogravimetric analysis (TGA). The surface hydrophobicity of the organic-inorganic nanocomposites was evaluated in terms of the surface contact angle analysis.

EXPERIMENTAL

Materials

Organic silanes (*i.e.*, phenyltrichlorosilane and dimethylchlorosilane) were purchased from Gelest Co., USA and used as received. Paraformaldehyde was obtained from Tokyo Kasei Kogyo Co., Japan. Platinum complex (Pt-dvs, 2 wt% Pt in toluene) was purchased from Aldrich Co., USA. Phenol, aniline, allyl glycidyl ether, hexaammoniate nickel (II) chloride $[Ni(NH_3)_6]Cl_2$, sodium hydroxide (NaOH), silver nitrate ($AgNO_3$) and magnesium sulfate ($MgSO_4$) were obtained from Shanghai Reagent Co., China. Before use, allyl glycidyl ether was distilled over CaH_2 under decreased pressure. Benzoxazine monomer, *i.e.,* bis(3-phenyl-3,4-dihydro-2H-1,3-benzoxazinyl) isopropane (denoted BZ) was synthesized by following the method of literature reported by Ishida *et al* [25]. Organic solvents such as pyridine, ethanol, methanol and toluene were obtained from commercial source. Before use, toluene and pyridine were distilled over calcium hydride (CaH_2) and then stored in a sealed vessel with the molecular sieve of 4 Å.

Synthesis of cis-Hexa(phenyl hydro) MOSS

First, the coordinate of the metals (*i.e.,* nickel/sodium) with phenylsiloxanolates was prepared *via* the reactions of polyphenylsilsesquioxane with sodium hydroxide (NaOH) and $[Ni(NH_3)_6]Cl_2$ by following the method of literature reported by Shchegolikhina *et al.* [14]. To a flask containing 400 mL of deionized water and 150 mL of toluene, phenyltrichlorosilane (100.000 g, 0.624 mol) dissolved in 100 mL of toluene was dropwise added within 30 min with vigorous stirring; the system was held in an ice-water bath. The organic layer was isolated and then the solvent was eliminated *via* rotary evaporation to afford the polyphenylsilsesquioxane. Thereafter, the as-obtained polyphenylsilsesquioxane (13.660 g, 0.1 mol with respect

of silicon) and NaOH (2.000 g, 0.05 mol) dissolved in 300 mL of *n*-butanol were added into a flask equipped with a magnetic stirrer; the mixture was refluxed with vigorous stirring until the homogenous solution was obtained and then sodium (1.150 g, 0.05 mol) was added at the temperature of 50 ~ 60 ^{o}C. The system was refluxed for 30 min and then hexaammoniate nickel (II) chloride $[Ni(NH_3)_6]Cl_2$ (11.590 g, 0.05 mol) were added. The reaction system was refluxed for additional 2 hours and the hot solution was filtered to eliminate NaCl precipitates and then *n*-butanol was removed *via* rotary evaporation. The mixture was recrystallized in hexane at -5 ^{o}C overnight and the yellow crystals were formed. After dried in a vacuum oven at 30 ^{o}C for one hour, the yellow crystals (8.100 g) (*i.e.,* nickel/sodium hexaphenylcyclohexasiloxanolate coordinate) were obtained with the yield of 84%.

Second, the above coordinate (8.480 g, 4.99 mol) was added to the mixture composed of anhydrous toluene (160 mL), dimethylchlorosilane $[(CH_3)_2SiHCl)]$ (42.000 g, 378.2 mmol) and pyridine (28.400 g, 307.2 mmol) at room temperature. The reaction was carried out at 25 ^{o}C for 24 hours with vigorous stirring. The mixture was filtered to remove the precipitates and the filtrate was washed with deionized water until no chlorine ions were detected with aqueous solution of silver nitrate ($AgNO_3$). After dried with anhydrous magnesium sulfate ($MgSO_4$), all the solvents were eliminated *via* rotary evaporation and the viscous liquid, *i.e., cis*-hexa[(phenyl)(dimethylsiloxy)]cyclohexasiloxane [denoted *cis*-hexa(phenyl hydro) MOSS] (7.360 g) was obtained with the yield of 97.0 %. ^{1}H NMR (400MHz, $CDCl_3$, 22 ^{o}C): 7.36 ~ 7.15 (*m*, 5H, $C_6\boldsymbol{H}_5$), 4.89 (*sept*, 1H, Si***H***), 0.30 [*d*, 6H, $Si(C\boldsymbol{H}_3)_2$]. ^{29}Si NMR (ppm, $CDCl_3$): -5.1, -5.4 and -81.4. MALDI-TOF-MS: 1200.2 Da (calculated: 1201.1 Da)

Synthesis of cis-Hexa(phenyl glycidyl) MOSS

Cis-Hexa[(phenyl)(demethylsiloxypropylglycidylether)cyclohexasiloxane [denoted *cis*-hexa(phenyl glycidyl) MOSS] was synthesized *via* the hydrosilylation between *cis*-hexa(phenyl hydro) MOSS and allyl glycidyl ether (AGE) as depicted in Scheme 1.To a flask equipped with a magnetic bar, *cis*-hexa(phenyl hydro) MOSS (1.180 g, 1.0 mmol), AGE (1.370 g, 12.0 mmol) and anhydrous toluene (10 mL) were charged with vigorous stirring; 5 μL of Karstdet catalyst was added with a syringe.

After purged with highly pure nitrogen for 30 min with vigorous stirrring, the reactive system was heated to 95 ^{o}C; the reaction was performed at this temperature for 36 hours to ensure the hydrosilylation to completion. The solvent and excess AGE were removed *via* rotary evaporation and a viscous liquid (1.860 g) was obtained with the yield of 96 %. ^{1}H NMR (400MHz, $CDCl_3$): 7.16 ~ 6.88 (*m*, 5H,$C_6\boldsymbol{H_5}$), 3.61, 3.28 (*m*, 2H, $SiCH_2CH_2CH_2OC\boldsymbol{H_2}$), 3.31 (*m*, 2H, $SiCH_2CH_2C\boldsymbol{H_2}O$), 3.09 [1H, C***H*** (epoxide)], 2.77, 2.57 [2H, C$\boldsymbol{H_2}$ (epoxide)], 1.52 (*m*, 2H, $SiCH_2C\boldsymbol{H_2}$), 0.54 (*m*, 2H, SiC$\boldsymbol{H_2}$), 0.17 (*s*, 6H, $Si(C\boldsymbol{H_3})_2$). ^{13}C NMR (100MHz, $CDCl_3$): 134.30, 133.472, 129.62 and 127.41 ($\boldsymbol{C_6}H_5$), 74.42 ($SiCH_2CH_2\boldsymbol{C}H_2O$), 71.56 [$\boldsymbol{C}H_2O$-$(CH_2)_3Si$], 51.07 [$OCH_2\boldsymbol{C}H$(epoxide)], 44.58 ($\boldsymbol{C}H_2$, epoxide), 23.57 ($SiCH_2\boldsymbol{C}H_2CH_2O$), 14.24 ($Si\boldsymbol{C}H_2CH_2CH_2O$), 0.60 [$Si(\boldsymbol{C}H_3)_2$]. MALDI-TOF-Mass: 1885.7Da (calculated: 1886.0 Da)

Preparation of Organic-inorganic Hybrids

To a glass beaker, desired amount of BZ and *cis*-hexa(phenyl glycidyl) MOSS were charged. To facilitate the mixing, a smallest amount of dichloromethane was added with vigorous stirring. The solvent was evaporated at room temperature and the residual solvent was removed *in vacuo* at 60 ^{o}C for 2 hours to afford the homogenous and transparent mixtures. The mixtures were poured into aluminum foils. The curing reaction was carried out at 190 ^{o}C for 4 hours. In this work, the hybrids with the content of *cis*-hexa(phenyl glycidyl) MOSS up to 30 wt% were prepared.

Techniques and Measurement

Nuclear Magnetic Resonance (NMR) Spectroscopy

The ^{1}H NMR measurement was carried out on a Varian Mercury Plus 400 MHz NMR spectrometer at 25 ^{o}C and the ^{29}Si NMR spectra were obtained on a Bruker Avance III 400 MHz NMR spectrometer. The samples were dissolved with deuterated chloroform ($CDCl_3$) and the solutions were measured with tetramethylsilane (TMS) as an internal reference.

Fourier Transform Infrared (FTIR) spectroscopy

The FTIR measurements were conducted on a Perkin-Elmer Paragon 1000 spectrometer at room temperature. The thermosetting samples were grounded into powder and the powder was mixed with KBr pellets to press into the small flakes for measurements. All the specimens were sufficiently thin to be within a range where the Beer-Lambert law is obeyed. In all cases 32 scans at a resolution of 2 cm^{-1} were used to record the spectra.

Matrix-Assisted Ultraviolet Laser Desorption / Ionization Time-of-Flight Mass Spectroscopy (MALDI-TOF-MS)

Gentisic acid (2,5-dihydroxybenzoic acid, DHB) was used as the matrix with dichloromethane as the solvent. The MALDI-TOF-MS experiment was carried out on an IonSpec HiResMALDI mass spectrometer equipped with a pulsed nitrogen laser (λ = 337 nm; pulse with = 3 ns). This instrument operated at an accelerating potential of 20 kV in reflector mode. Sodium is used as the cationizing agent and all the data shown are for positive ions.

Differential Scanning Calorimetry (DSC)

DSC measurements were performed on a TA Instruments Q2000 differential scanning calorimeter in a dry nitrogen atmosphere. The instrument was calibrated with a standard indium. To investigate the non-isothermal curing kinetics, the specimens were heated from 150 to 300 °C at five different heating rates of 2, 5, 10, 15 and 20 °C /min, respectively.

Thermal Gravimetric Analysis (TGA)

A TA Instruments Q5000 thermal gravimetric analyzer was used to investigate the thermal stability of the samples. The measurements were conducted in nitrogen atmosphere from ambient temperature to 800 ^{o}C at the heating rate of 20 ^{o}C min^{-1}. The temperature of initial degradation (T_d) was taken as the onset temperature of initial degradation (T_d) at which 5 wt% of weight loss occurs.

Dynamic Mechanical Thermal Analysis (DMTA)

Dynamic mechanical tests were carried out on a TA instruments DMA Q800 dynamic mechanical thermal analyzer (DMTA) equipped with a liquid nitrogen apparatus in a single cantilever mode. The frequency used was 1.0 Hz, and the heating rate of 3.0 ^{o}C/min was used. The specimen dimension was 25 × 5.0 × 1.75 mm^3. The experiments were carried out from 0 to 300 ^{o}C.

Scanning Electron Microscopy (SEM)

The thermosets were fractured under cryogenic condition using liquid nitrogen. The fracture surfaces were coated with thin layers of gold of about 100 Å. The specimens were examined with an FEI Inspect S50 scanning electron microscope (SEM) at an activation voltage of 5 kV. Qualitative and semi-quantitative chemical analysis in the model of energy-dispersive X-ray spectroscopy (EDX) was performed with a ThermoNORAN model (Quest model) spectrometer.

Transmission Electronic Microscopy (TEM)

The thermosets were trimmed using a microtome machine; the thickness of the specimens is about 70 nm. Then the ultrathin sections were placed on 200 mesh copper grids for observation. Transmission electron microscopy analyses were performed on a JEOL JEM-2010 high-resolution transmission electron microscopy at an acceleration voltage of 120 kV.

Surface Contact Angle Analysis

In order to prepare the specimens for contact angle measurements, both BZ and *cis*-hexa(phenyl glycidyl) MOSS were dissolved with dichloromethane at the concentration of 20 wt%. The solutions were spin-coated onto glass slides at the rate of 2000 r/m and the thickness of films was controlled to about 20 μm. The solvent was slowly evaporated at room temperature and the residual solvent was eliminated *in vacuo* for 48 hours before the mixtures were cured at 190 °C for 4 hours. The flat and free surfaces of the thermosets were then obtained and used for the measurement of

contact angles. The static contact angle measurements were carried out on a KH-01-2 contact angle measurement instrument (Beijing Kangsente Scientific Instruments Co., China) at room temperature with ultrapure water and ethylene glycol as probe liquids, respectively.

RESULT AND DISCUSSION

Synthesis of cis-Hexa(phenyl glycidyl) MOSS

The route of synthesis for *cis*-hexa[(phenyl)(dimethylsiloxypropylglycidylether) cyclohexasiloxane [denoted *cis*-hexa(phenyl glycidyl) MOSS] is shown in Scheme 1. First, the coordinate of the metals (*i.e.,* nickel/sodium) with phenylsiloxanolates was prepared *via* the reaction of polyphenylsilsesquioxane with sodium hydroxide (NaOH) and hexaammoniate nickel (II) chloride ($[Ni(NH_3)_6]Cl_2$) by following the method of literature reported by Shchegolikhina *et al.* [14]. It was reported that the crystal of the coordinate consisted of stereoregular phenyl macrocycles coordinated to alkaline and/or the transitional metal (*viz.* nickel). The crystal displayed a sandwich structure, in which the metal atoms were positioned in a plane between two layers of cyclosiloxanolate fragments and the six-$SiO_{3/2}$-membered organosiloxanolate ligands [*i.e,* $phenylSi(O)O^{-1}]_6$ were in all-*cis* configuration, which were fixed by Ni(II) ions. For the purpose of structural analysis, the coordinate was ever allowed to react with trimethlychlorosilane, vinyldimethylchlorosilane and chloromethyldimethylsilane to afford the corresponding MOSS derivatives [14]. In this work, this metallacyclosiloxanolate was used to react with dimethylchlorosilane to afford a macrocyclic oligomeric silsesquioxane (MOSS) macromer bearing six Si-H bonds [denoted *cis*-hexa(phenyl hydro) MOSS]. It is expected that *cis*-hexa(phenyl hydro) MOSS can further be functionalized into various derivatives *via* hydrosilylation reaction. In this work, the hydrosilylation reaction of *cis*-hexa(phenyl hydro) MOSS with allyl glycidyl ether (AGE) was carried out to obtain *cis*-hexa[(phenyl)(demethylsiloxypropylglycidylether)cyclohexasiloxane [denoted *cis*-hexa(phenyl glycidyl) MOSS].

Shown in Figure 1 is the ^{29}Si NMR spectrum of *cis*-hexa(phenyl hydro) MOSS. Two peaks of silicon resonance were detected at -4.4 and -80.3 ppm, respectively. The former is assignable to the silicon nucleus bonded with hydrogen

atom (*i.e.,* that in Si-H bond) whereas the latter to the silicon nucleus of macrocyclic silsesquioxane backbones. These two resonance peaks indicate that the compound had a macrocyclic structures with silsesquioxane as the backbone and with hydrodimethylsiloxyl side groups. It should be pointed out that the baseline uplifting of the spectral line in the range of -75 to -100 ppm resulted from the resonance of ^{29}Si nucleus in the NMR tube. This compound was subjected to MALDI-TOF-MS spectroscopy to measure its molecular weight and its mass spectrum was shown in Figure 2. A group of intense peaks centered at the value of M/Z to be 1200.2 were detected, implying that the compound possessed the molecular weight of 1177.2 Da. The molecular weight was exactly identical with the value estimated according to its structural formula (*viz.* $C_{48}H_{72}Si_{12}O_9$). The ^{29}Si NMR and MALD-TOF-MS spectroscopy indicates that *cis*-hexa(phenyl hydro) MOSS was successfully obtained.

The hydrosilylation reaction of *cis*-hexa(phenyl hydro) MOSS with allyl glycidyl ether (AGE) was carried out to afford *cis*-hexa(phenyl glycidyl) MOSS. Shown in Figure 3 are the FTIR spectra of *cis*-hexa(phenyl hydro) MOSS and *cis*-hexa(phenyl glycidyl) MOSS. *cis*-Hexa(phenyl hydro) MOSS is characteristic of the bands in the range of 958 ~ 1204 and 2134 cm^{-1}; the former is assignable to the stretching vibration of Si-O-Si linkage whereas the latter to Si-H bonds. With the occurrence of hydrosilylation reaction, the band at 2134 cm^{-1} completely disappeared whereas the latter remained almost unchanged. Concurrently, there appeared a new band at 910 cm^{-1}, which is assignable to the stretching vibration of epoxide groups. The FTIR spectroscopy indicate that the hydrosilylation reaction between *cis*-hexa(phenyl hydro) MOSS and AGE was successfully carried out. Shown in Figure 4 is the ^{1}H NMR spectra of *cis*-hexa(phenyl hydro) MOSS and *cis*-hexa(phenyl glycidyl) MOSS. For the *cis*-hexa(phenyl hydro) MOSS, the resonance signals of the protons assignable to Si-H bonds and phenyl protons were detected at 4.74 and 6.8 ~ 7.8 ppm, respectively. With the occurrence of hydrosilylation, notably, the signal of resonance at 4.74 ppm, assignable to the protons of Si-H bonds completely disappeared. Concurrently, there appeared several new signals of resonance at 0.55, 1.51, 2.56, 2.78, 3.09, 3.32 and 3.60 ppm, which are attributable to the protons of methylene groups in propyl glycidyl ether moiety as indicated in Figure 4. This compound was also subjected to MALDI-TOF-MS spectroscopy to measure its molecular weight. As shown in Figure 5, a group of intense peaks centered at the value

of M/Z to be 1885.7 were detected, implying that the compound possessed the molecular weight of 1862.7 Da. The molecular weight is exactly identical with the value estimated according to its structural formula (*viz.* $C_{84}H_{138}Si_{12}O_{21}$). The ^{1}H NMR, MALD-TOF-MS and FTIR spectroscopy indicates that *cis*-hexa(phenyl glycidyl) MOSS was successfully obtained.

Formation of Organic-inorganic Nanocomposites

The above functional MOSS macromer was incoporated into polybenzoxazine (PBZ) to prepare the organic-inorganic composites. All the mixtures of BZ monomer with *cis*-hexa(phenyl glycidyl) MOSS were homogenous and transparent, suggesting that both of monomers were miscible and no phase separation occured at the scale exceeding the wavelength of visible lights. These mixtures were subjected to the curing reaction at 190 ^{o}C for 4 hours to obtain the thermosetting composites.The organic-inorganic composites were prepared with the content of *cis*-hexa(phenyl glycidyl) MOSS up to 30 wt%. All the hybrid composites are homogenous and tranparent, suggesting that no reaction-induced phase separation occured in the process of curing reaction. The morphology of the hybrid composites was further investigated by means of transmission electron microscopy (TEM) and scanning electron microscopy (SEM). Rpresentatuively shown in Figure 6 is the TEM image of the PBZ thermoset containing 30 wt% of *cis*-hexa(phenyl glycidyl) MOSS. The featureless morphology was displayed without a sign of microphase separation. To confirm the homogenous dispersion of the MOSS macromer in PBZ matrix, the organic-inorganic composites were further subjected to morphological observation by means of scanning electron microscopy (SEM). Representatively shown in Figure 7 are the SEM micrographs of the composite containing 20 wt% of *cis*-hexa(phenyl glycidyl) MOSS. The featureless morphology was also exhibted (See Figure 7A), which was in good agreement with the TEM results. In this work, the distribution of silicon element in the thermosets was further investigated with EDX technique. Shown in Figure 7B is the mapping image of silicon element. Notably, the silicon element was homogenously dispersed in the PBZ matrix, *i.e.,* no aggragation at the micrometer scale occurred. The results of both TEM and SEM indicates that the macrocylic silsesquioxane blocks were homogenously dispersed in the PBZ matrix at the segmental level, *i.e.,* the

organic-inorganic nanocomposites were successfully obtained.

It is proposed that there was the inter-component reaction between PBZ network and *cis*-hexa(phenyl glycidyl) MOSS (Scheme 2). In the PBZ network, there were a great number of phenolic hydroxyl groups, whhich were created *via* the thermally induced ring-opening polymerization of BZ monomer. Phenolic hydroxyl groups are capable of reacting with glycidyl groups at elevated temoerature [41]. In this case, the inter-component reaction between PBZ and *cis*-hexa(phenyl glycidyl) MOSS would result in the formation of the addtional crosslinking between PBZ network and the MOSS macromer. The inter-component reaction was readily investigated by means of FTIR spectroscopy whereas the additional crosslinking density can be reflected by examining the glass transition temperatures (T_g's) of the organic-inorganic nanocomposites. Shown in Figure 8 are the FTIR spectra of BZ, *cis*-hexa(phenyl glycidyl) MOSS, PBZ and the organic-inorganic nanocomposites containing *cis*-hexa(phenyl glycidyl) MOSS in the range of 4000 ~ 400 cm^{-1}. For BZ monomer, the absorption band at 945 cm^{-1} is assignable to the streching vibration of oxazine ring. For *cis*-hexa(phenyl glycidyl) MOSS, the bands at 910 and 1057 cm^{-1} are assignable to the stretching vibration of epoxide group and Si-O-Si bonds in the MOSS macromer, respectively. For plain PBZ and the organic-inorganic nanocomposites, the bands at 945 cm^{-1} completely dissapeared, indicating that the curing reaction was carried out to completion. Cocurently, there appeared the bands at 1057 cm^{-1}, the intensity of which increased with increasing the content of *cis*-hexa(phenyl glycidyl) MOSS. The FTIR spectroscopy showed that the resulting thermosets combined the structural features from PBZ and the MOSS macromer. It is of interest to note that the band at 910 cm^{-1} assignable to epoxide groups of the MOSS macromer virtually diappeared. This observation suggests that all the epoxide groups of the MOSS macromers reacted with the phenolic hydroxyl groups.

The curing behavior of the organic-inorganic composite system was investigated in terms of non-isothermal curing kinetics by means of differential scanning calorimetry (DSC). Plain BZ and its mixtures with *cis*-hexa(phenyl glycidyl) MOSS were heated from 150 to 300 °C at the different heating rates of 2, 5, 10, 15 and 20 °C/min. Shown in Figure 9 are the DSC thermographs of BZ and its mixture containing 20 wt% of *cis*-hexa(phenyl glycidyl) MOSS. For plain BZ, a single exothermic peak was displayed at each heating rate. The exothermic peak resulted

from the ring-opening polymerization of BZ monomer. In contrast, each exothermic peak of the hybrid mixture was composed of multiple components, implying that there could be additional reactions involved with the curing process. Herewith, we define the onset (T_i) and peak (T_p) temperatures to account for the starting and maximum temperatures of each exothermic peak, respectively. The values of heat of reaction (ΔH), T_i and T_p of the curing reaction are summarized in Table 1. It is seen that the T_i's and T_p's increased with increasing the heating rates. The exothermic peaks of curing reaction increasingly became increasingly sharp with increasing the heating rates. Notably, the hybrid mixture displayed higher T_i, and T_p than plain BZ at the identical heating rate, implying that the curing reaction of the hybrid mixture occurred at the temperature higher than plain BZ. Then enhanced curing temperature is attributable to the dilution effect of *cis*-hexa(phenyl glycidyl) MOSS. For plain BZ, the heat of reaction is about ΔH = 310 J/g. Notably, the incorporation of *cis*-hexa(phenyl glycidyl) MOSS caused the depression in the heat of reaction, indicative of the dilution effect of the MOSS macromer.

In this work, we estimated the activation energy of the curing reactions for plain BZ and the hybrid mixtures by using the above data of non-isothermal DSC scans. Kissinger and Ozawa approaches can be employed toward this end [42,43]. The Kissinger equation [42] can be represented by the eq. (1):

$$\ln\left(\frac{\beta}{T_p^2}\right) = \ln\left(\frac{Q_p AR}{E_a}\right) - \frac{E_a}{RT_p} \quad (1)$$

where β is the heating rate and T_p is the temperature of exothermic maximum. E_a is activation energy, R is the universal gas constant and A is the pre-exponential factor. Q_p is defined as:

$$Q_p = -[df(\alpha)/d\alpha]_{\alpha=\alpha_p} \quad (2)$$

where α is the extent of the reaction (conversion degree), $f(\alpha)$ is the differential conversion function depending on the reaction mechanism [44]. For the curing reaction of thermosets, this approach assumes that the extent of the reaction at the temperature of exothermic peak is constant, independent of heating rates. The activation energy (E_a) of reaction can be determined according to the linear plot of the logarithm of β/T_p^2 *versus* the inverse of the peak temperature of the exothermic curing reaction. The Ozawa method [43] is another approach of dynamic curing kinetics

without assuming any model. Its general expression can be represented by eq. (3):

$$\ln \beta = \ln\left(\frac{AE_a}{R}\right) - \ln F(\alpha) - 5.331 - 1.052\left(\frac{E_a}{RT}\right) \quad (3)$$

F(α) is a constant function and defined as:

$$F(\alpha) = \int_0^{\alpha} \frac{d\alpha}{f(\alpha)} \quad (4)$$

The plots of the logarithm of β/T_p^2 or β versus the reversal of the exothermic peak temperature are shown in the Figure 10. The good linear relationships for both the Kissinger and the Ozawa methods were obtained for plain BZ and its mixtures with *cis*-hexa(phenyl glycidyl) MOSS, suggesting that the validity of the two approaches. From the slopes of the linear plots, the activation energy values were thus calculated and also summarized in Table 1. For plain BZ, the E_a values were obtained to be 112.4 and 114.6 kJ/mol for Kissinger and Ozawa approaches, respectively. Notably, the E_a values of the mixtures of BZ with *cis*-hexa(phenyl glycidyl) MOSS were significantly lower than values of BZ monomer. For instance, the E_a values were obtained to be 90.1 and 93.4 kJ/mol for the mixture containing 20 wt% of *cis*-hexa(phenyl glycidyl) MOSS. It is noted that in the range of composition investigated, this mixture exhibted the minimun of the activation energy. The decreased E_a values suggest that the incoporation of *cis*-hexa(phenyl glycidyl) MOSS faciliated the curing reaction of BZ. It is proposed that there were two opposite tendencies to affect the curing reaction in the composite system. On the one hand, the MOSS macromer was capable of reacting with PBZ through the reaction between epoxide groups and phenolic hydroxyl groups. This reaction was favorable for the curing reaction of BZ since the cured product was comsumed with this reaction. On the other hand, *cis*-hexa(phenyl glycidyl) MOSS exerted a dilution effect on the ring-opening polymerization of BZ monomer. It is plausible to propose that the apparent E_a values reflected the collective contribution. As a consequence, the mixture containing 20 wt% of *cis*-hexa(phenyl glycidyl) MOSS displayed the minimun Ea values among the samples investigated.

Thermomechanical Properties

Dynamic Mechanical Thermal Analysis

Plain PBZ and the organic-inorganic nanocomposites were subjected to dynamic mechanical thermal analysis (DMTA) and the DMTA spectra are showed in Figure 11. For plain PBZ, one α peak was exhibited at 177 ^{o}C, attributable to the glass-rubber transition of the crosslinked polymer. Up incorporating *cis*-hexa(phenyl glycidyl) MOSS, the α transitions were observed to shift to higher temperatures, depending on the content of *cis*-hexa(phenyl glycidyl) MOSS. For the nanocomposites containing 5, 10, 20 and 30 wt% of *cis*-hexa(phenyl glycidyl) MOSS, the T_g's were measured to be 216, 224, 193 and 179 ^{o}C, respectively (See Table 2). Notably, the nanocomposite containing 10 wt% of *cis*-hexa(phenyl glycidyl) MOSS displayed the T_g as high as 224 ^{o}C. The following factors could affect the glass transition behaviro of the organic-inorganic hybrids: i) the nanoreinforcement of the rigid macrocyclic silsesquioxanes on PBZ network, ii) the formation of the additional crosslinking between PBZ network and the MOSS macomer and iii) the untight packing of the PBZ chains owing to the incoporation of the bulk MOSS macromer. The first two would give rise to the increase in T_g's of the thermosets whereas the last gave rise to the decrease in T_g's. The results of TEM and SEM showed that the macrocylic silsesquioxanes were homogeneously dispersed into PBZ matrix at the segmenal scale. These inorganic building blocks couls restrict the motion of the macromolecular chains and thus gave rise to the enhancement of T_g. Such an effect has been realized as the nanoreinforcement in a vareity of POSS-containing nanocomposites [2-5]. The inter-component reaction resulted in the increase in crosslinking density of the PBZ networks. Therefore, the T_g's of the organic-inorganic nanocomposites were increased owing to the increased crosslinking density. Nonetheless, the incoporation of the bulky macrocyclic silsesquioxanes into the PBZ network would also affect the tight packing of the macromolecular chains. The bulky and rigid macrocyclic silsesquioxanes with an all-*cis* configuration in place of PBZ chains could result that the PBZ chains failed densely to pack, *i.e.,* the free volume was increased. The increased free volume was responsible for the depression in glass transition temperatures. It is noteworthy that the T_g's of the organic-inorganic nanocomposites did not monotonously increase with increasing the content of the MOSS macromer; the maximum of T_g's (*c.a.* 224 ^{o}C) appeared while the nanocomposite contained 10 wt% of *cis*-hexa(phenyl glycidyl) MOSS. This observation can be well interpreted in terms of the collective contribution of the above three factors. Also shown in Figure 11 are the plots of dynamic storage

moduli as functions of temperature for plain PBZ and the nanocomposites containing *cis*-hexa(phenyl glycidyl) MOSS. In the glassy state the dynamic storage moduli of the organic-inorganic nanocomposite were slightly lower than that of plain PBZ. With incorporation of the MOSS macromer into the PBZ network, the moduli of the organic-inorganic nanocomposites could be changed owing to the following factors: i) the nanoreinforcement of the macrocyclic silsesquioxane on PBZ matrix, ii) the increased crosslinking density owing to the inter-component reaction between PBZ and the MOSS macromer and iii) the decreased density of the thermosets owing to the inclusion of the bulky silsesquioxane macrocycles. The first two factors gave rise to the increased modulus of the materials whereas the last to the depression. The restriction of MOSS on PBZ chains as well as the formation of the additional crosslinking between PBZ and the MOSS macromer was evidenced by the increased glass transition temperatures of the organic-inorganic nanocomposites compared to plain PBZ. On the other hand, the bulky, macrocyclic silsesquioxane in place of macromolecular segments resulted that the macromolecular chains were unable densely to pack, *i.e.,* the decreased density of the materials could give rise to the decrease in the moduli of the materials. It is plausible to propose that the moduli of the organic-inorganic nanocomposites in the glassy state reflected the combined contributions from the above factors. More importantly, the organic-inorganic nanocomposites displayed the dynamic mechanical properties quite different from plain PBZ in views of the storage modulus of the materials in the rubbery state. Under the present condition of DMTA measurements, we failed to observe the rubbery plateau of plain PBZ owing to the relatively low crosslinking density of this thermoset (Figure 11). In marked contrast to plain PBZ, the organic-inorganic nanocomposites displayed stable rubbery plateaus in the plots of storage modulus as functions of temperature while the content of *cis*-hexa(phenyl glycidyl) MOSS was 10 wt% or higher. This observation can be interpreted on the basis of: i) the formation of the additional crosslinking between PBZ and the MOSS macromer and ii) the nanoreinforcement of silsesquioxane macrocycles on PBZ networks.

Thermogravimetric Analysis

Thermogravimetric analysis (TGA) was used to investigate the thermal stability

of the organic-inorganic nanocomposites. The TGA curves of plain PBZ and the nanocomposites are shown in Figure 12 and the results of TGA are summarized in Table 3. Notably, all the samples displayed similar degradation profiles, suggesting that the inclusion of the MOSS macromer did not significantly alter the degradation mechanism of the materials. For plain PBZ, the initial decomposition occurred at *c.a.* 310 ^{o}C and the char yield was *c.a.* 23 % at 800 ^{o}C. For the organic-inorganic nanocomposites, the initial decomposition temperatures (T_d's) and the yields of degradation residues were much higher than those of the control PBZ. The T_d's increased with increasing the concentration of *cis*-hexa(phenyl glycidyl) MOSS. While the content of *cis*-hexa(phenyl glycidyl) MOSS was 30 wt%, the T_d and the yield of degradation residue were measured to be *c.a.* 334 ^{o}C and 36.5%, respectively. The yield of degradation residue was significantly higher than the theoretical yields of ceramic estimated according to the contents of *cis*-hexa(phenyl glycidyl) MOSS. Therefore, it is judged that there was a synergism between the organic and inorganic components in the process of degradation. It has been proposed that the chemical linkage between organic and inorganic components was crucial to the improvement in thermal stabilities of organic-inorganic nanocomposites [45,46]. In this system, the MOSS macromers participated in the formation of the crosslinked network, *i.e.*, the silsesquioxane macrocycles were bonded into PBZ networks. The macrocyclic silsesquioxanes in place of PBZ chains are favorable to the suppression of the mass loss from segmental decomposition *via* gaseous fragments.

Surface Contact Angle Analysis

As an organosilicon compound, the MOSS macromer possessed low surface free energy [47-52]. It is expected that the surface hydrophobicity (or dewettability) of PBZ thermoset would be significantly improved with the inclusion of the inorganic component. The improved surface hydrophobicity would result from the enrichment of the organosilicon component at the surface of the organic-inorganic nanocomposites. This effect can be readily examined by means of the measurement of contact angles. In this work, the flat and free surfaces of plain PBZ and its nanocomposites containing the MOSS macromer were created for the measurement of contact angles. The static surface contact angles were measured with water and ethylene glycol as probe liquids, respectively; the results of the measurements are

summarized in Table 3. For plain PBZ thermoset, the water contact angle was measured to be *c.a.* 80.3°. The relatively low value of the water contact angle suggests that plain PBZ was quite hydrophilic. Compared to plain PBZ thermoset, the water contact angles of the organic-inorganic nanocomposites were significantly enhanced; the values of water contact angles increased with increasing the content of the MOSS macromer (See Figure 13). While the content of *cis*-hexa(phenyl glycidyl) MOSS, the surface contact angle was measured to be 91.1°, which was much higher than that of plain PBZ. While the content of *cis*-hexa(phenyl glycidyl) MOSS was 10 wt% or higher, the values of the water contact angles of the nanocomposites were quite close, suggesting that the surfaces of the nanocomposites were enriched to saturation by the organosilicon component (*viz.* MOSS). For the nanocomposite containing 30 wt% of *cis*-hexa(phenyl glycidyl) MOSS, the water contact angle was measured to be as high as 98.3°, indicating that the surface hydrophobicity was significantly enhanced. The enhanced values of surface contact angles were attributable to the enrichment of the organosilicon component (*viz.* MOSS) at the surface of the composites.

The surface free energies of the organic-inorganic copolymers were calculated according to the geometric mean model [53-55]:

$$\cos\theta = \frac{2}{\gamma_L}\left[(\gamma_L^d \gamma_s^d)^{\frac{1}{2}} + (\gamma_L^p \gamma_s^p)^{\frac{1}{2}}\right] - 1 \quad (1)$$

$$\gamma_s = \gamma_s^d + \gamma_s^p \quad (2)$$

where θ is contact angle and γ_L is the liquid surface tension; γ_s^d and γ_s^p the dispersive and polar components of γ_L, respectively. From Table 2, it is seen that with increasing the content of *cis*-hexa(phenyl glycidyl) MOSS, the total surface free energy of the copolymers was reduced from 31.0 to 15.9 mN/m. Both of the polar and dispersive values were quite sensitive to the concentration of *cis*-hexa(phenyl glycidyl) MOSS, suggesting that the MOSS blocks have been significantly enriched onto the surface energy of the materials, *i.e.*, the silsesquioxane macrocycles on the surface of the organic-inorganic behaved as the screening agent to enhance the surface hydrophobicity.

CONCLUSION

In this work, we successfully synthesized *cis*-hexa[(phenyl)(dimethyl siloxypropylglycidylether)cyclohexasiloxane, a novel stereoregular macrocyclic oligomeric silsesquioxane. This MOSS macromer has been characterized by means of ^{29}Si, ^{1}H NMR and MALD-TOF-MS spectroscopy. The MOSS macromer was incorporated into polybenzoxazine (PBZ) thermosets and the organic-inorganic nanocomposites were obtained. The results of SEM and TEM showed that the macrocyclic silsesquioxane was dispersed into PBZ matrices at the segmental level. Dynamic mechanical thermal analysis (DMTA) and thermogravimetric analysis (TGA) showed that the organic-inorganic nanocomposites displayed enhanced glass transition temperatures (T_g's) and thermal stability compared to the plain PBZ thermoset. The improved thermomechanical properties are attributable to the reinforcement of MOSS macrocycles on the PBZ matrix and the additional crosslinking between PBZ and the MOSS macromer. The results of static contact angle measurement showed that the surface hydrophobicity of the organic-inorganic nanocomposites was significantly improved compared to the plain PBZ thermoset.

ACKNOWLEDGMENT

The financial supports from Natural Science Foundation of China (No. 51133003, 21274091 and 21304058) were gratefully acknowledged.

REFERENCES

1. M. G. Voronkov and V. I. Lavrent'yev, *Top. Curr. Chem.*, 1982, **102**, 199.
2. J. J. Schwab and J. D. Lichtenhan, *Appl. Organomet. Chem.*, 1998, **12**, 707.
3. G. Li, L. Wang, H. Ni and C. U. Pittman Jr, *J. Inorganic. Organomet. Polym.*, 2002, **11**, 123.
4. Y. Abe and T. Gunji, *Prog. Polym. Sci.*, 2004, **29**, 149.
5. S. H. Phillips, T. S. Haddad and S. J. Tomczak, *Curr. Opin. Solid State Mater. Sci.*, 2004, **8**, 21.
6. R. M. Laine, *J. Mater. Chem.*, 2005, **15**, 3725.
7. P. D. Lickiss and F. Rataboul, *Adv. Organomet. Chem.*, 2008, **57**, 1.

8. R. M. Laine and M. F. Roll, *Macromolecules*, 2011, **44**, 1073.

9. S.-W. Kuo and F.-C. Chang, *Prog. Polym. Sci.*, 2011, **36**, 1649.

10. O. I. Shchegolikhina, V. A. Igonin, Y. A. Molodtsova and Y. A. Pozdnyakova, *J. Organomet. Chem.*, 1998, **562**, 141.

11. N. V. Sergienko, E. S. Trankina, V. I. Pavlov, A. A. Zhdanov, K. A. Lyssenko and M. Y. Antipin, *Russ. Chem. Bull. Int. Ed.*, 2004, **53**, 351.

12. Y. A. Molodtsova, Y. A. Pozdnyakova, K. A. Lyssenko, I. V. Blagodatskikh, D. E. Katsoulis and O. I. Shchegolikhina, *J. Organomet. Chem.*, 1998, **571**, 31.

13. O. I. Shchegolikhina, Y. A. Pozdnyakova, S. D. Molodtsova and B. Korkin, *Organometallics*, 2000, **19**, 1077.

14. O. I. Shchegolikhina, Y. A. Pozdnyakova, Y. A. Molodtsova, S. D. Korkin, S. S. Bukalov, L. A. Leites, K. A. Lyssenko, A. S. Peregudov, N. Auner and D. E. Katsoulis, *Inorg. Chem.*, 2002, **41**, 6892.

15. Y. A. Pozdnyakova, K. A. Lyssenko, I. V. Blagodatskikh, N. Auner, D. E. Katsoulis and O. I. Shchegolikhina, *Eur. J. Inorg. Chem.*, 2004, **2004**, 1253.

16. O. I. Shchegolikhina, A. A. Zhdanov, V. A. Igonin, Y. E. Ovchinnikov, V. E. Shklover and Y. T. Struchkov, *Organomet. Chem. USSR.*, 1991, **4**, 39.

17. V. A. Igonin, S. V. Lindeman, Y. T. Struchkov, Y. A. Molodtsova, Y. A. Pozdniakova, O. I. Shchegolikhina and A. A. Zhdanov, *Russ. Chem. Bull.*, 1993, **42**, 176.

18. J. Han and S. Zheng, *Macromolecules*, 2008, **41**, 4561.

19. J. Han and S. Zheng, *J. Polym. Sci, Part A: Polym. Chem.*, 2009, **47**, 6894.

20. J. Han, L. Zhu and S. Zheng, *Euro. Polym. J.*, 2012, **48**, 730.

21. L. Zhu, C. Zhang, J. Han, S. Zheng and X. Li, *Soft Matter*, 2012, **8**, 7062.

22. Y. Yi, L. Li and S. Zheng, *Polymer*, 2014, **55,** , 3925.

23. Y. Yi and S. Zheng, *RSC Adv.*, 2014, **4**, 28439.

24. H. Ishida and T. Agag, *Handbook of Benzoxazine*, Elsevier, Amsterdam, 2011.

25. X. Ning and H. Ishida, *J. Polym. Sci., Part A: Polym. Chem.*, 1994, **32**, 1121.

26. H. J. Kim, B. Zdenka and H. Ishida, *Polymer*, 1999, **40**, 1815.

27. H. D. Kim, Z. Brunovska and H. Ishida, *Polymer*, 1999, **40**, 6565.

28. H. Ishida and Y.-H. Lee, *Polymer*, 2001, **42**, 6971.

29. H. Ishida and Y.-H. Lee, *J. Polym. Sci, Part B: Polym. Phys.*, 2001, **39**, 736.

30. T. Takeichi, T. Agag and R. Zeidam, *J. Polym. Sci, Part A: Polym. Chem.*, 2001, **39**, 2633.

31. T. Agag and T. Takeichi, *Macromolecules*, 2001, **34**, 7257.

32. T. Tekeichi, R. Zeidam and T. Agag, *Polymer*, 2002, **43**, 45.

33. T. Agag, H. Tsuchiya and T. Takeichi, *Polymer*, 2004, **45**, 7903.

34. Y.-J. Lee, S.-W. Kuo, Y.-C. Su, J.-K. Chen, C.-W. Tu and F.-C. Chang, *Polymer*, 2004, **45**, 6321.

35. Y.-C. Su, W.-C. Chen, K.-L. Ou and F-C. Chang, *Polymer*, 2006, **46**, 3758.

36. Y.-J. Lee, S.-W. Kuo, C.-F. Huang and F.-C. Chang, *Polymer*, 2006, **4**, 4378.

37. N. N. Ghosh, B. Kiskan and Y. Yagci, *Prog. Polym. Sci.*, 2007, **32**, 1344.

38. P. Velez-Herrera, K. Doyama, H. Abe and H. Ishida, *Macromolecules*, 2008, **41**, 9704.

39. H. Ishida and Y.-H. Lee, *Polym. & Polym. Compos.*, 2001, **9**, 121.

40. R. Xu, L. Wang and D. Yu, in *Handbook of Benzoxazine*, (Ed. H. Ishida and T. Agag), Elsevier, Amsterdam, 2011, pp. 517~539.

41. Y. Liu and S. Zheng, *J. Polym. Sci.: Part A: Polym. Chem.*, 2006, **44**, 1168.

42. H. F. Kissinger, *Anal. Chem.,* 1957, **29**, 1702

43. T. J. Ozawa, *Therm. Anal.* 1970, ***2***, 301

44. C. Jubsilp, S. Damrongsakkul, T. Takeichi, S. Rimdusit, T*hermochim Acta*, 2006, ***447,*** 131.

45. J. Choi, J. Harcup, A. F. Yee, Q. Zhu and R. M. Laine, *J. Am. Chem. Soc.*, 2001, **123**, 11420.

46. J. Choi, S. G. Kim and R. M. Laine, *Macromolecules*, 2004, **37**, 99.

47. W. J. Feast, H. S. Munro and R. W. Richarsa, *Polymer Surface and Interface, II*, John Wiley & Sons, Chichester, 1993.

48. P. A. V. O. R. Muisener, C. A. Jalbert, C. Yuan, J. Baetzold, R. Mason, D. Wong, Y. J. Kim, J. T. Koberstein and B. Gunesin, *Macromolecules*, 2003, **36**, 2956.

49. J. T. Koberstein, *J. Polym. Sci. Part B: Polym. Phys.*, 2004, **42**, 2942.

50. S. Turri and M. Levi, *Macromolecules*, 2005, **38**, 5569.

51. S. Turri and M. Levi, *Macromol. Rapid. Commun.*, 2005, **26**, 1233.

52. M. Oaten and N. R. Choudhury, *Macromolecules*, 2005, **38**, 6392.

53. D. H. Kaelble, *J. Adhes.*, 1970, **2**, 66.

54. D. H. Kaelble, *Phys. Chem. of Adhesion*, Wiley-Interscience, New York, 1971.

55. W. Damson, *Physical Chemistry of Surfaces*, Wiley-Interscience, New York, 1990.

Table 1. Data of non-isothermal DSC curing kinetics for plain PBZ and the nanocomposites containing 5, 10, 20, 30 wt% of *cis*-hexa(phenyl glycidyl) MOSS

MOSS* (wt%)	β (^{o}C/min)	T_i (^{o}C)	T_p (^{o}C)	ΔH (J/g)	E_a (Kissinger) (kJ/mol)	E_a (Ozawa) (kJ/mol)
0	2	163.1	201.6	297.7	112.1	114.6
	5	183.5	212.2	306.4		
	10	196.7	222.7	312.0		
	15	208.2	231.4	311.3		
	20	217.5	240.5	316.6		
5	2	177.2	200.1	273.1	92.9	96.1
	5	195.3	218.8	268.4		
	10	210.8	230.8	263.6		
	15	218.5	240.9	263.0		
	20	227.1	247.0	262.5		
10	2	180.1	201.9	243.8	90.0	93.8
	5	195.6	220.4	244.7		
	10	211.1	234.2	246.5		
	15	219.5	244.3	243.1		
	20	227.3	250.2	245.4		
20	2	178.6	201.6	250.2	90.1	93.4
	5	197.5	224.3	238.6		
	10	213.3	233.6	242.5		
	15	226.7	245.0	241.9		
	20	230.6	250.6	244.2		
30	2	189.1	210.8	230.5	105.4	108.2
	5	203.9	224.1	245.2		
	10	216.4	237.4	224.8		
	15	226.1	246.3	223.5		
	20	234.8	253.5	219.1		

*: MOSS stands for *cis*-hexa(phenyl glycidyl) MOSS

Table 2 Glass transition temperatures and thermal stability of plain PBZ and its nanocomposites containing *cis*-hexa(phenyl glycidyl) MOSS.

cis-Hexa(phenyl glycidyl) MOSS (wt%)	T_g (°C) [a]	T_d (°C)[b]	Residue (wt%)[c]
0	177	224	23.7
5	215	324	30.3
10	224	331	32.6
20	193	330	33.0
30	178	334	36.5

a: Values of DMTA at 1.0 Hz and the heating rate of 3.0 °C/min.

b: Temperature at mass loss of 5 wt% under nitrogen atmosphere.

c: Residue of degradation at 800 °C in nitrogen atmosphere.

Table 3 Static contact angles and surface free energy of plain PBZ and the nanocomposites containing *cis*-hexa(phenyl glycidyl) MOSS

MOSS (wt%)	Static contact angle (^{o})		Surface free energy (mN/m)		
	Θ_{water}	$\Theta_{ethylene\ glycol}$	γ^{d}_{s}	γ^{p}_{s}	γs
0	80.3 ± 0.5	54.2 ± 0.8	23.1	7.9	31.0
5	91.1 ± 0.7	76.2 ± 0.6	10.0	8.6	18.6
10	94.9 ± 0.4	78.8 ± 0.5	11.1	6.2	17.3
20	97.5 ± 0.6	81.0 ± 0.7	11.3	5.0	16.3
30	98.3 ± 0.5	81.9 ± 0.4	11.1	4.8	15.9

Water: γ_L=72.8 mN/m, γ^{d}_{L} = 21.8 mN/m, γ^{p}_{L} = 51.0 mN/m; Ethylene glycol: γ_L = 48.3 mN/m, γ^{d}_{L} = 29.3 mN/m, γ^{p}_{L} = 19.0 mN/m [55].

SCHEMES

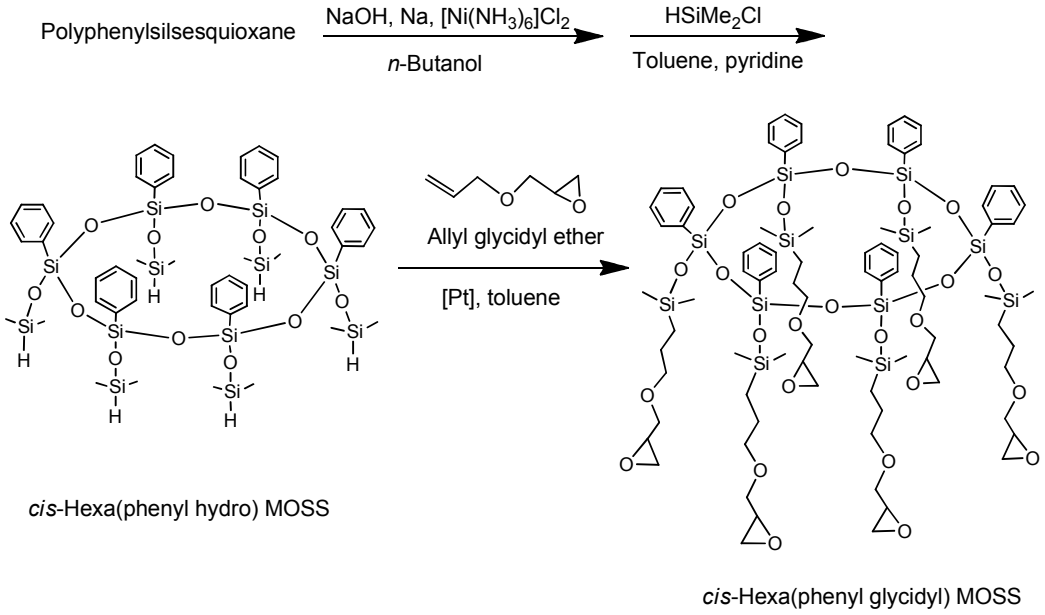

Scheme 1 Synthesis of *cis*-hexa(phenyl glycidyl) MOSS

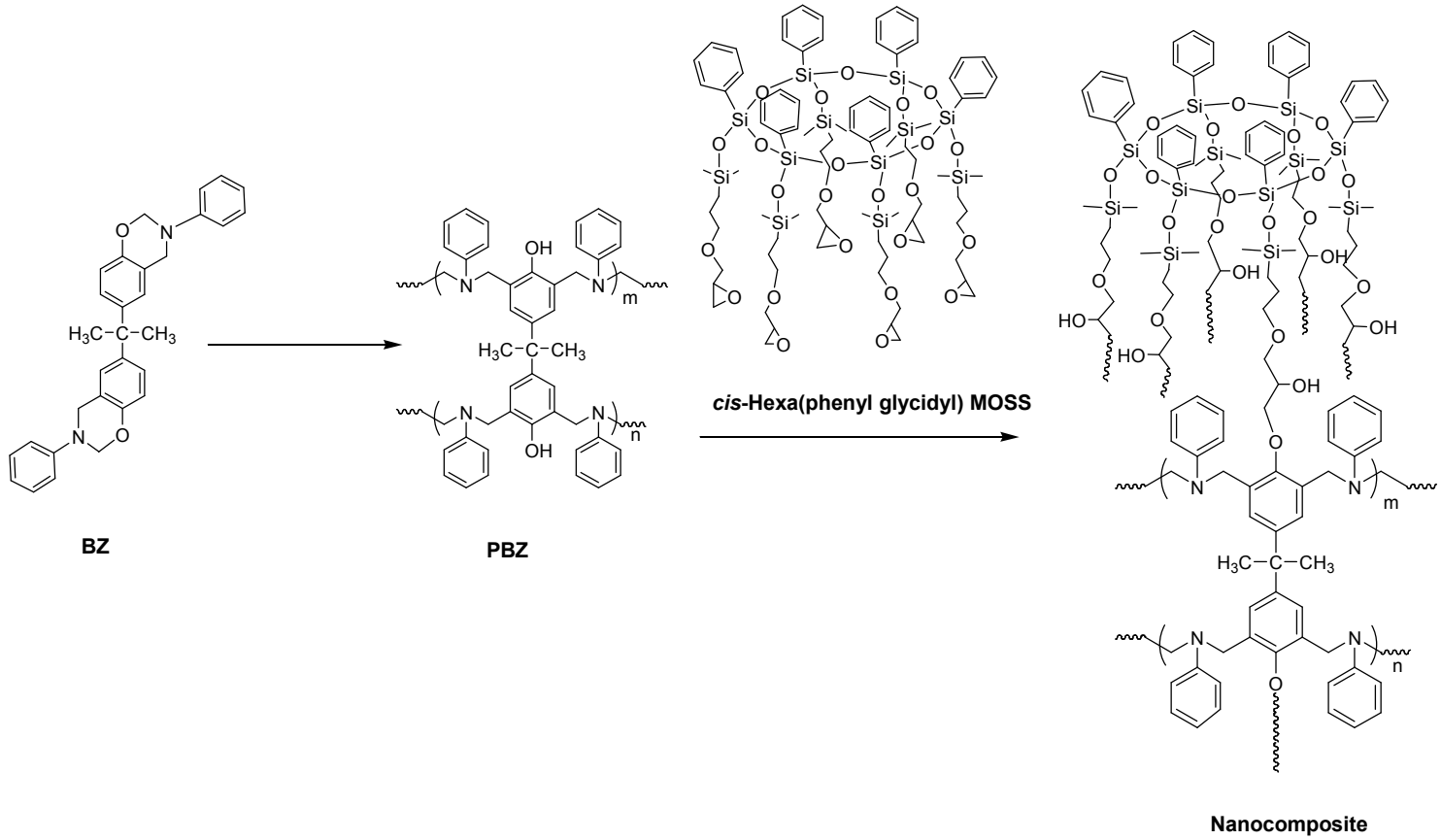

Scheme 2 Synthesis of the organic-inorgabnic PBZ nanocomposites containing *cis*-hexa(phenyl glycidyl) MOSS.

FIGURE CAPTIONS

Figure 1. ^{29}Si NMR spectrum of *cis*-hexa(phenyl hydro) MOSS;

Figure 2. MALDI-TOF-Mass spectrum of *cis*-hexa(phenyl hydro) MOSS;

Figure 3. FTIR spectra of: (A) *cis*-hexa(phenyl hydro) MOSS and (B) *cis*-hexa(phenyl glycidyl) MOSS;

Figure 4. ^{1}H NMR spectra of *cis*-hexa(phenyl hydro) and *cis*-hexa(phenyl glycidyl) MOSS;

Figure 5. MALDI-TOF-Mass spectrum of *cis*-hexa(phenyl glycidyl) MOSS;

Figure 6. TEM micrograph of the nanocomposite containing 30 wt% of *cis*-hexa(phenyl glycidyl) MOSS.

Figure 7. Morphological observation of the nanocomposite containing 20 wt% of *cis*-hexa(phenyl hydro) MOSS by means of scanning electron microscopy: A) SEM micrograph and B) Si element mapping image with EDX technique;

Figure 8. FTIR spectra of: A) BZ, B) *cis*-hexa(phenyl glycidyl) MOSS and the nanocomposites containing 30 wt% (C), 20 wt% (D), 10 wt% (E), 5 wt% (F) and 0 wt% (G) of *cis*-hexa(phenyl glycidyl) MOSS;

Figure 9. Non-isothermal DSC curves at different heating rates: Up) BZ; Dow) the BZ mixture containing 20 wt% of *cis*-hexa(phenyl glycidyl) MOSS.

Figure 10. Kissinger and Ozawa plots for the determination of E_a values: Up) BZ; Down) the BZ mixture containing 20 wt% of *cis*-hexa(phenyl glycidyl) MOSS.

Figure 11. DMTA curves of PBZ and the nanocomposites containg *cis*-hexa(phenyl glycidyl) MOSS;

Figure 12. TGA curves of PBZ and the organic-inorganic nanocomposites containg *cis*-hexa(phenyl glycidyl) MOSS;

Figure 13. Plot of surface water contact angles as a function of the content of *cis*-hexa(phenyl glycidyl) MOSS in the nanocomposites.

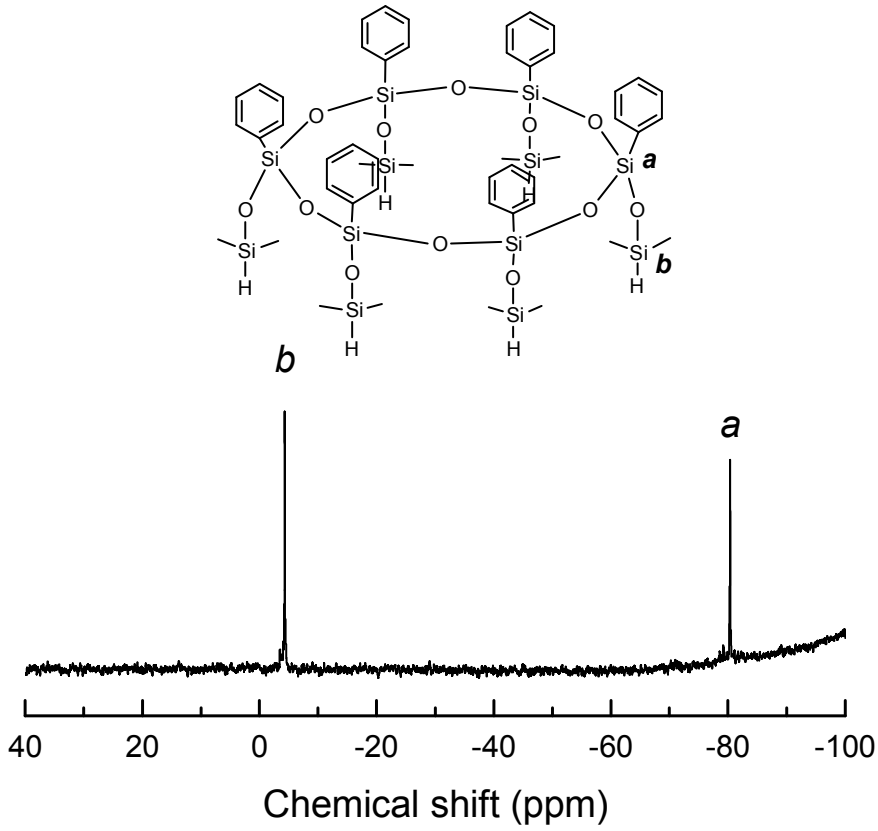

Figure 1

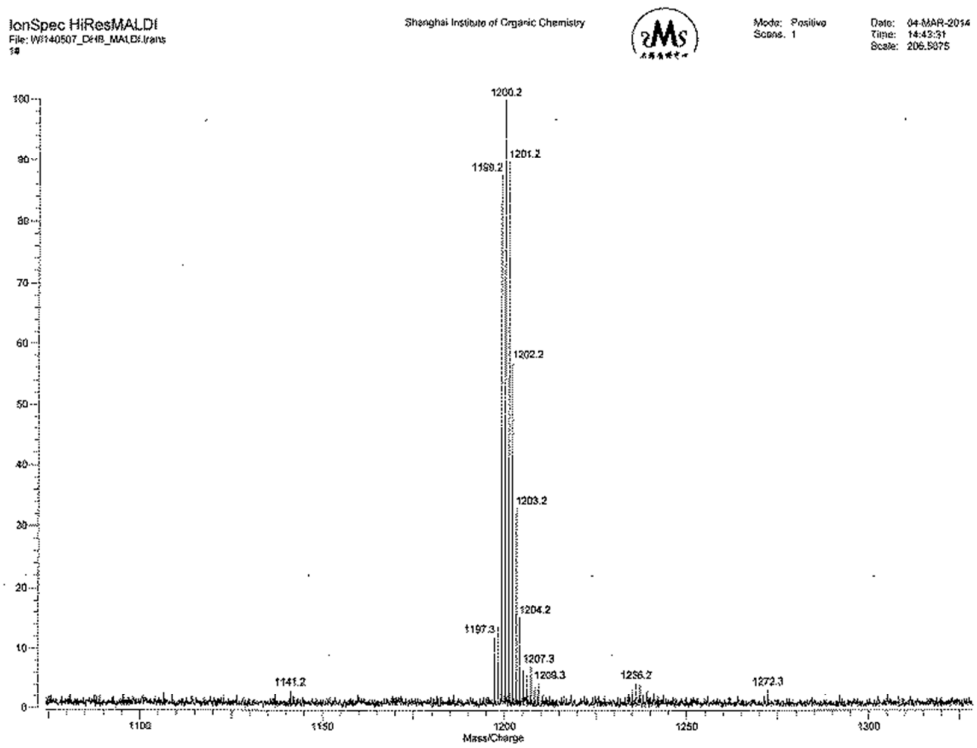
IonSpec HiResMALDI
File: W0140507_DHB_MALDI.trans
1#
Shanghai Institute of Organic Chemistry
Mode: Positive
Scans: 1
Date: 04-MAR-2014
Time: 14:43:31
Scale: 206.5075
1200.2
1201.2
1199.2
1202.2
1203.2
1204.2
1197.3
1207.3
1209.3
1256.2
1272.3
1141.2
100
90
80
70
60
50
40
30
20
10
0
1100
1150
1200
1250
1300
Mass/Charge

Figure 2

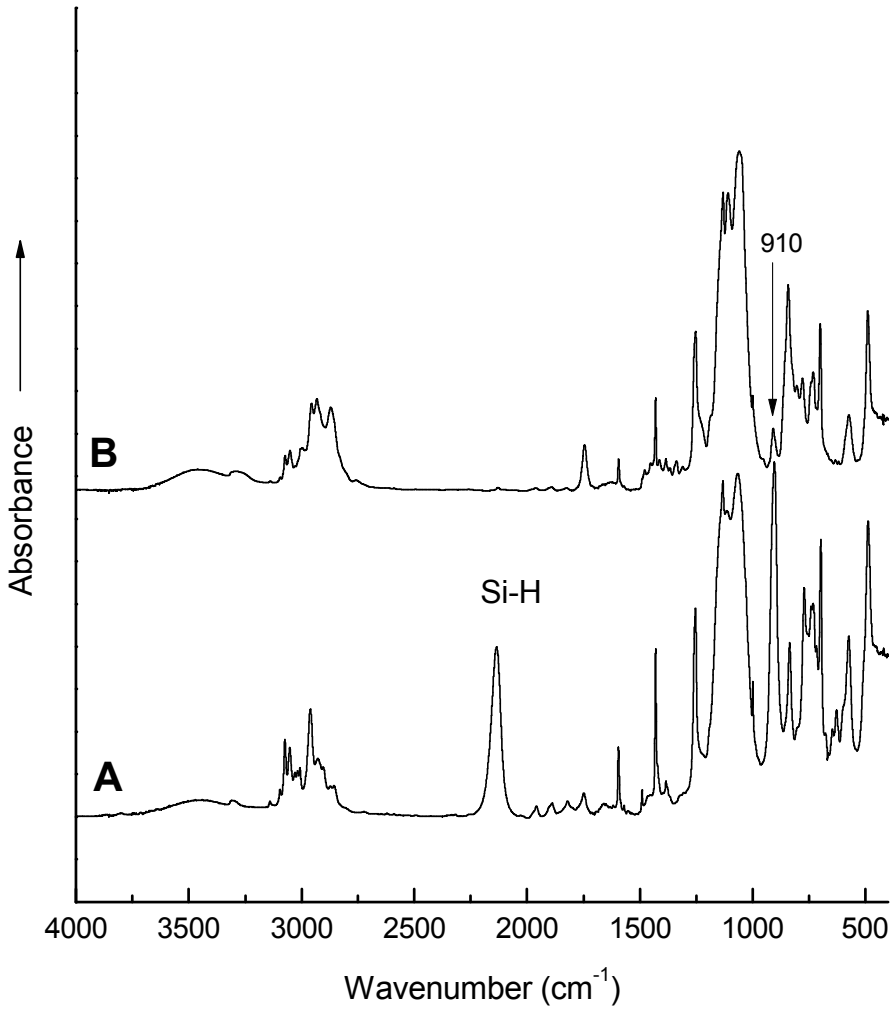
910
B
Absorbance
Si-H
A
4000
3500
3000
2500
2000
1500
1000
500
Wavenumber (cm-1)

Figure 3

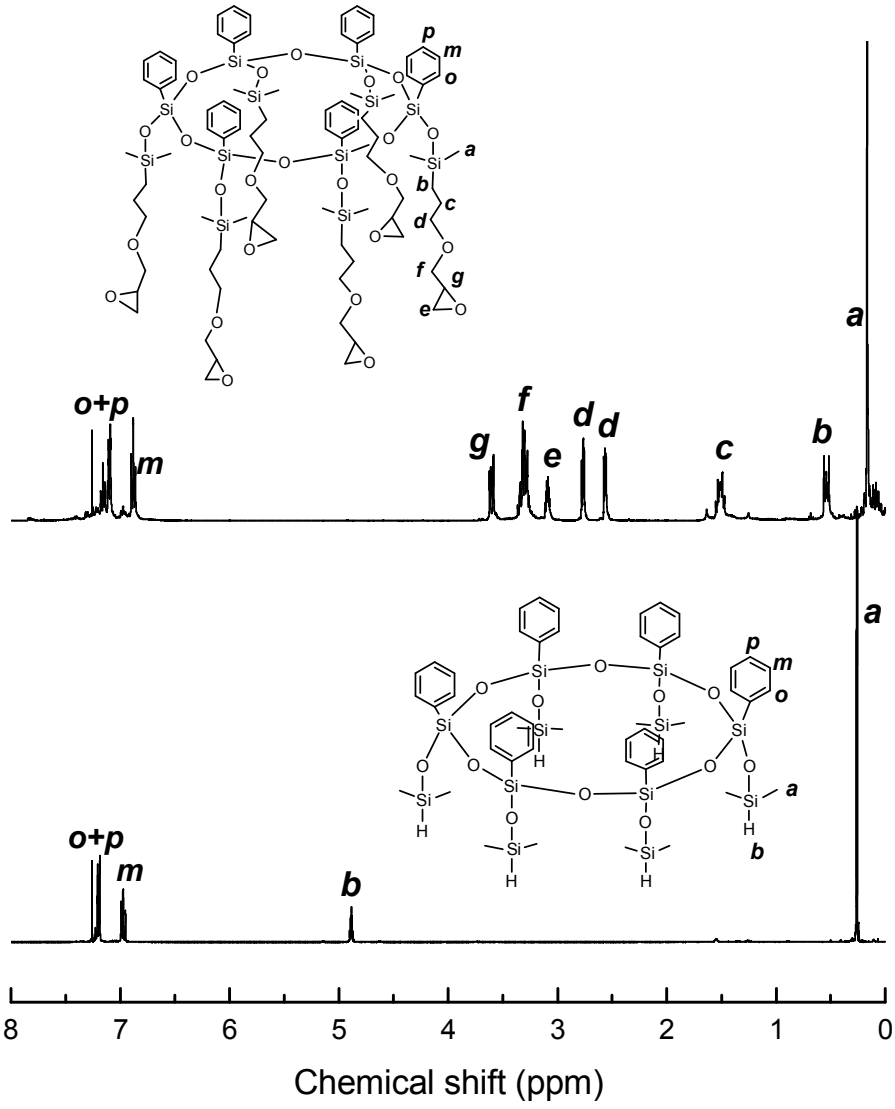
p
m
o
a
b
c
d
f
g
e
o+p
m
g
f
e
d
d
c
b
a
o+p
m
b
a
8
7
6
5
4
3
2
1
0
Chemical shift (ppm)

Figure 4

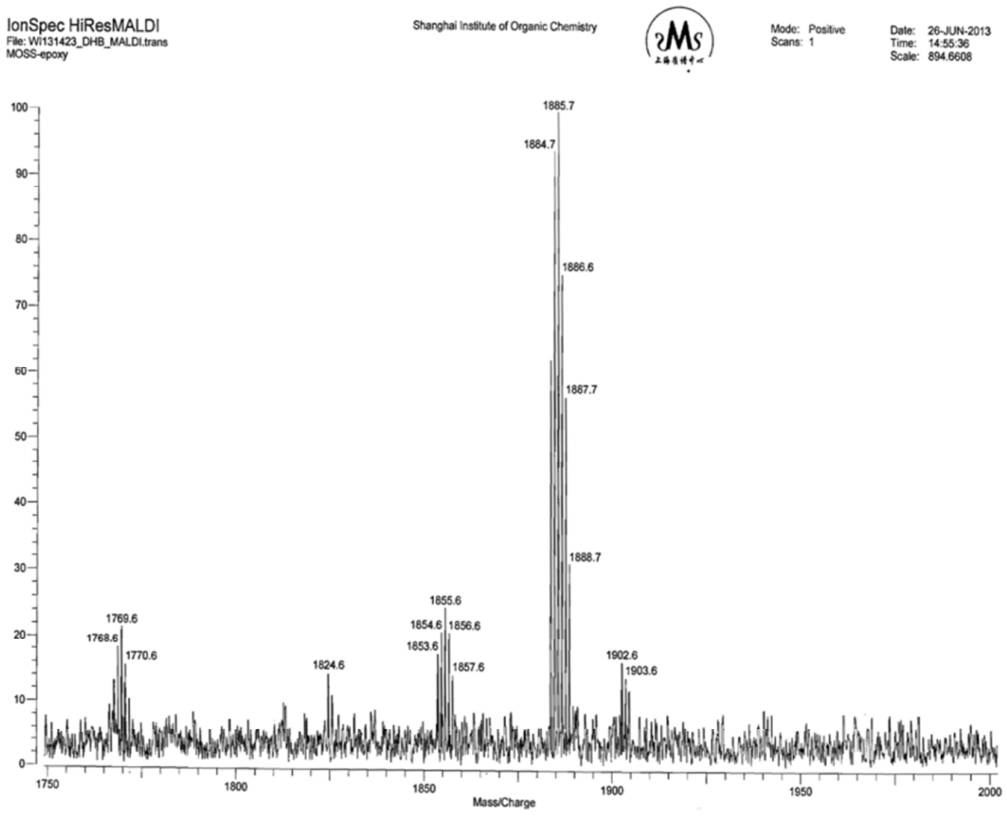
IonSpec HiResMALDI
File: Wi131423_DHB_MALDI.trans
MOSS-epoxy
Shanghai Institute of Organic Chemistry
Mode: Positive
Scans: 1
Date: 26-JUN-2013
Time: 14:55:36
Scale: 894.6608
1885.7
1884.7
1886.6
1887.7
1888.7
1855.6
1854.6
1856.6
1853.6
1857.6
1769.6
1768.6
1770.6
1824.6
1902.6
1903.6
Mass/Charge

Figure 5

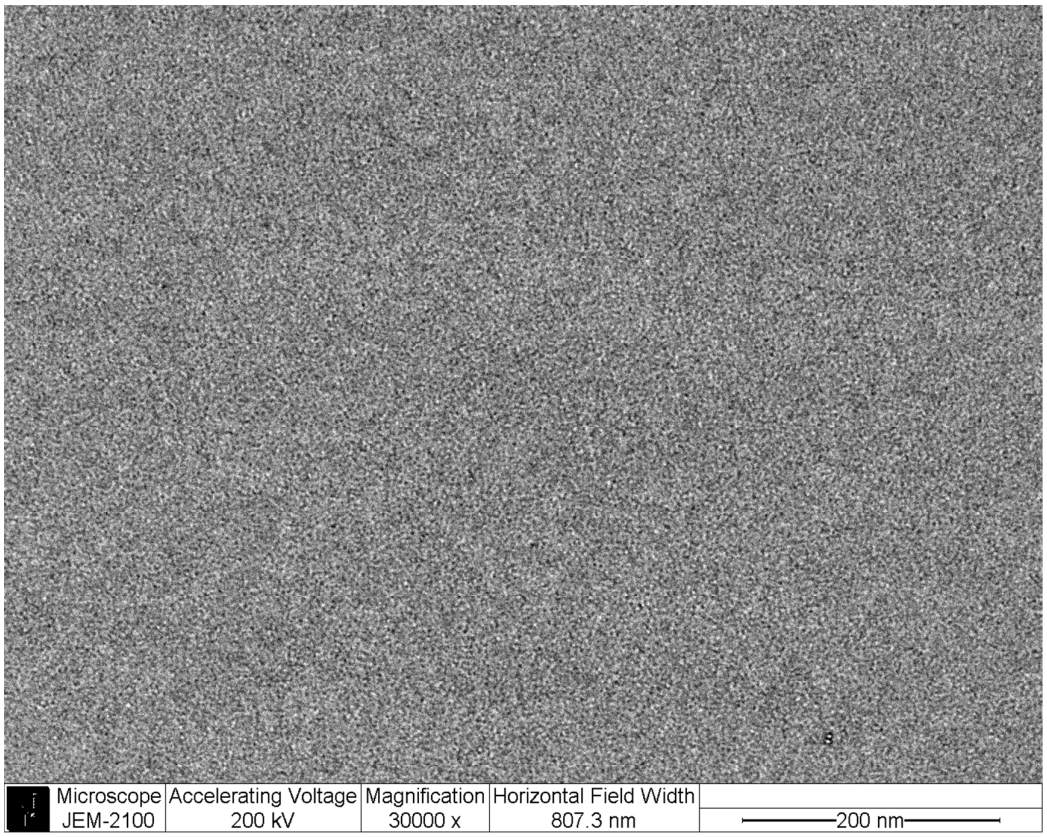
Microscope
JEM-2100
Accelerating Voltage
200 kV
Magnification
30000 x
Horizontal Field Width
807.3 nm
200 nm

Figure 6

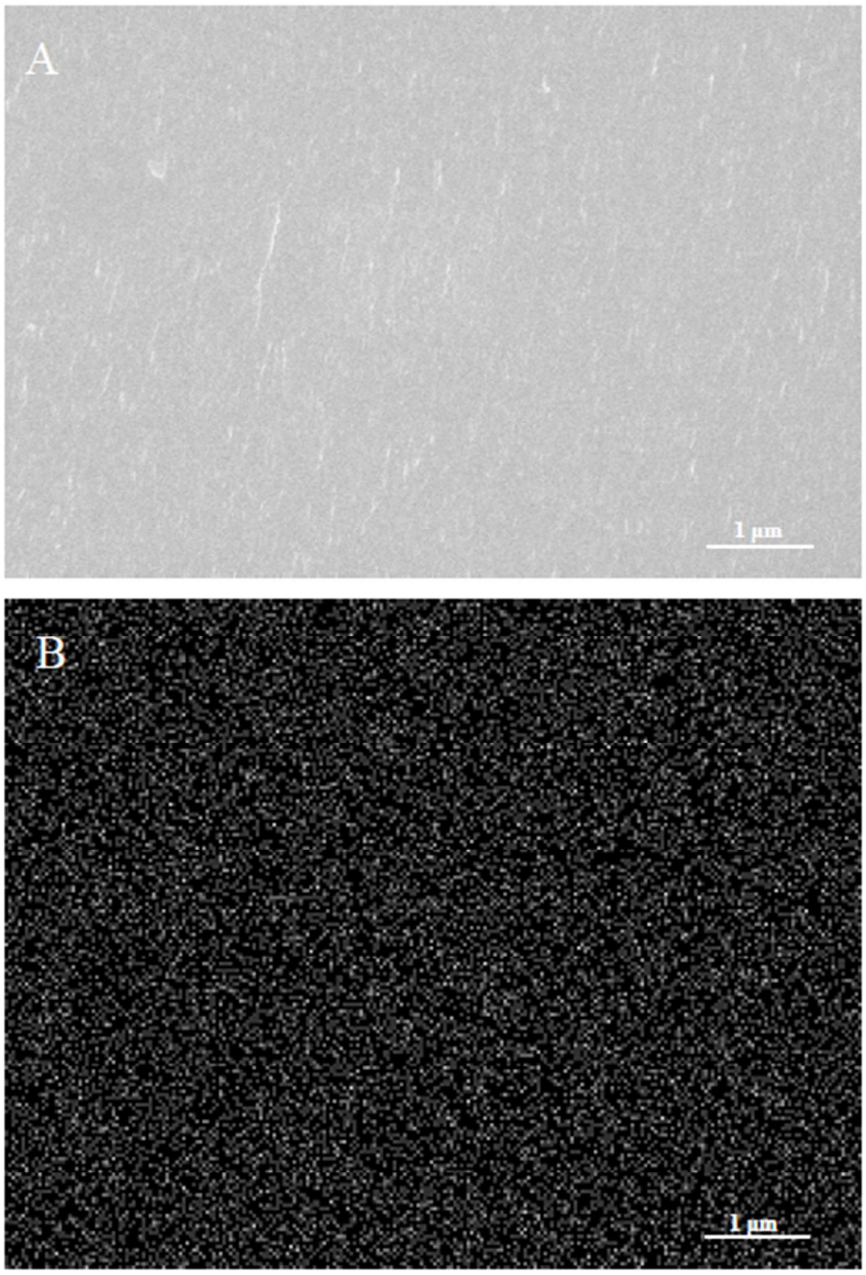

Figure 7

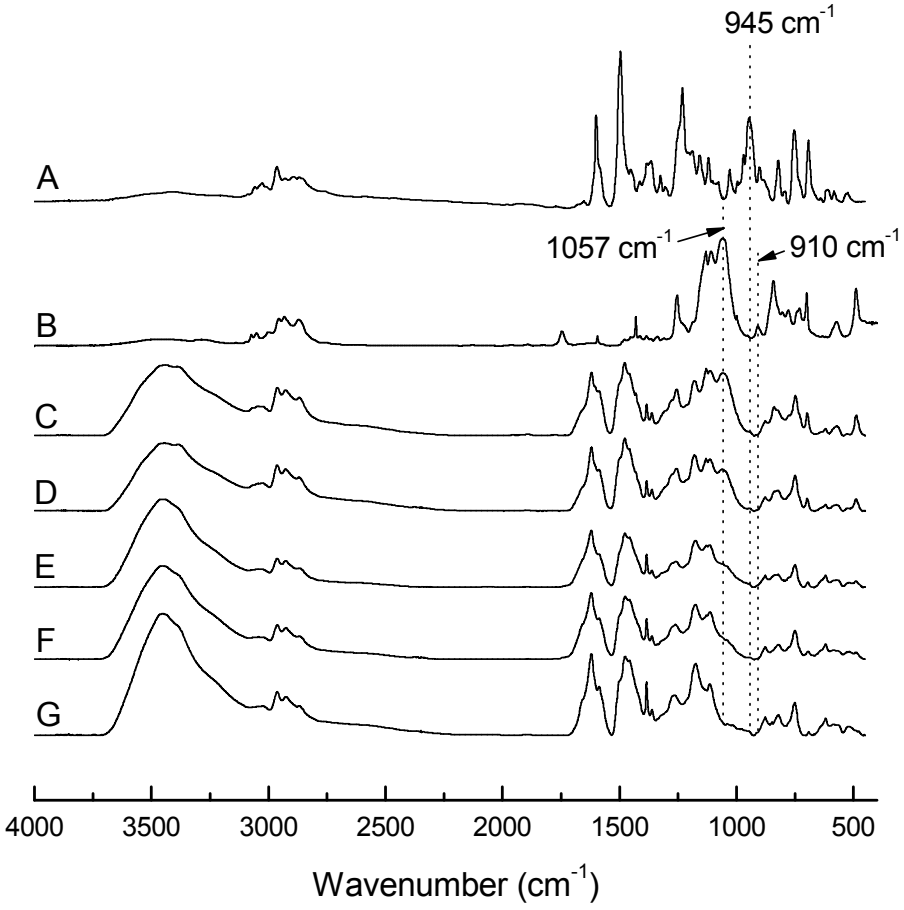
945 cm-1
A
1057 cm-1
910 cm-1
B
C
D
E
F
G
4000
3500
3000
2500
2000
1500
1000
500
Wavenumber (cm-1)

Figure 8

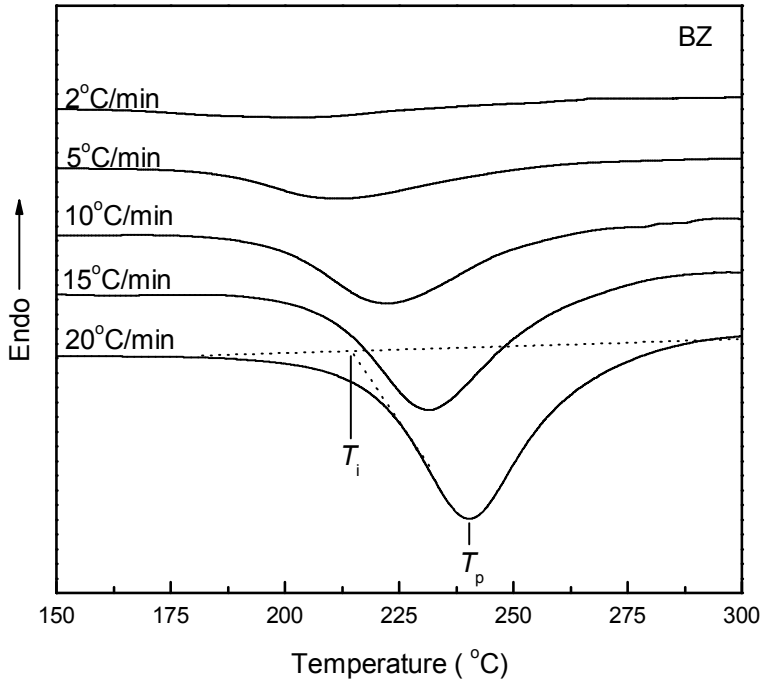
BZ
2°C/min
5°C/min
10°C/min
15°C/min
20°C/min
Endo
T_i
T_p
150
175
200
225
250
275
300
Temperature (°C)

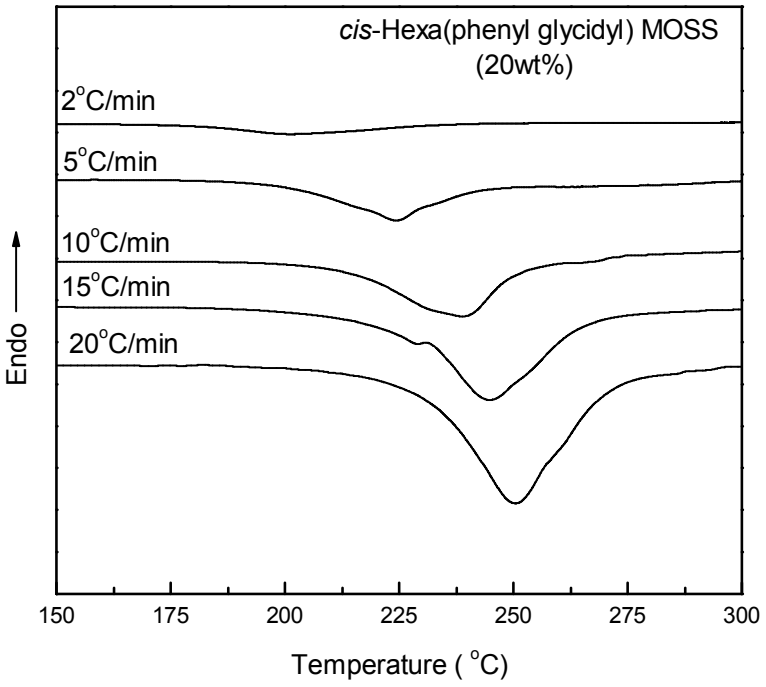
cis-Hexa(phenyl glycidyl) MOSS
(20wt%)
2°C/min
5°C/min
10°C/min
15°C/min
20°C/min
Endo
150
175
200
225
250
275
300
Temperature (°C)

Figure 9

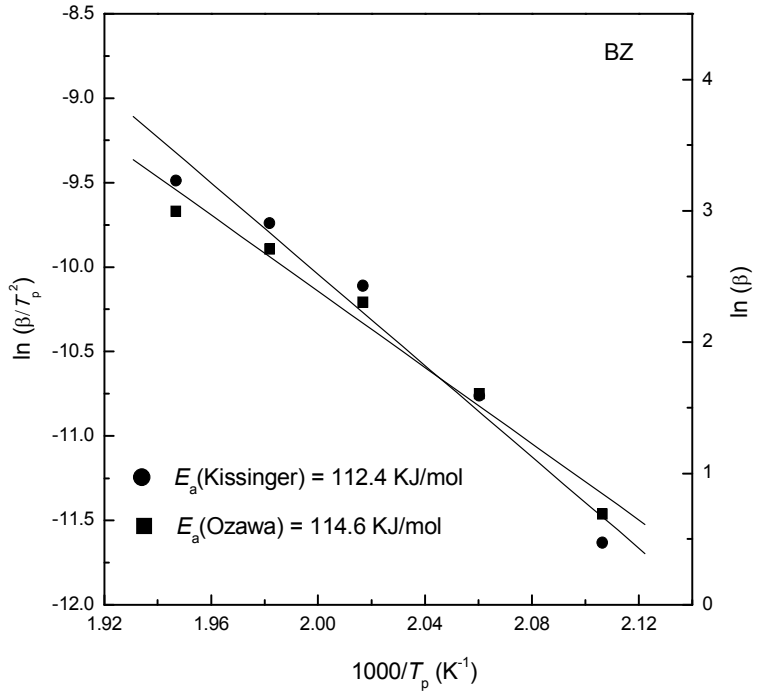
BZ
E_a(Kissinger) = 112.4 KJ/mol
E_a(Ozawa) = 114.6 KJ/mol
ln (β/T_p^2)
ln (β)
1000/T_p (K^{-1})

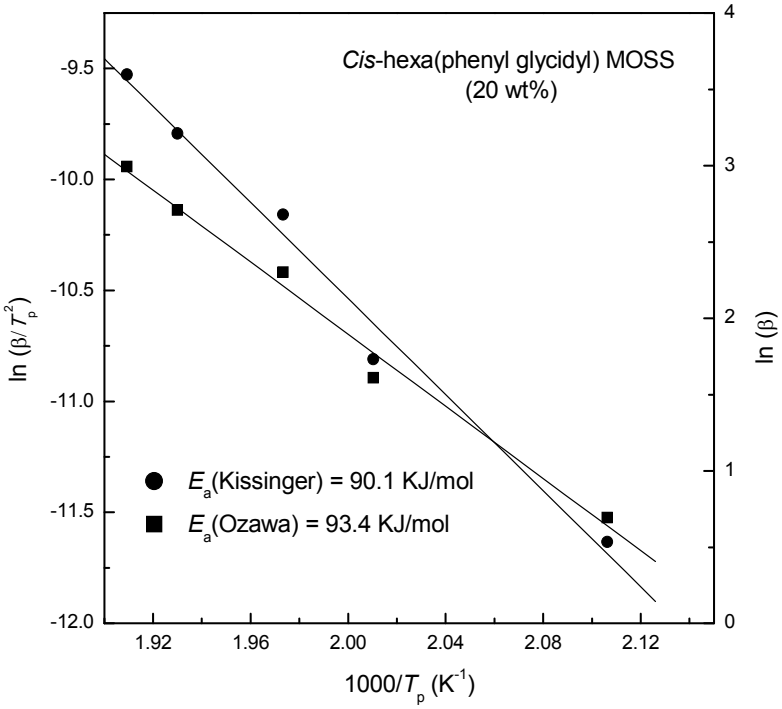
Cis-hexa(phenyl glycidyl) MOSS
(20 wt%)
E_a(Kissinger) = 90.1 KJ/mol
E_a(Ozawa) = 93.4 KJ/mol
ln (β/T_p^2)
ln (β)
1000/T_p (K^{-1})

Figure 10

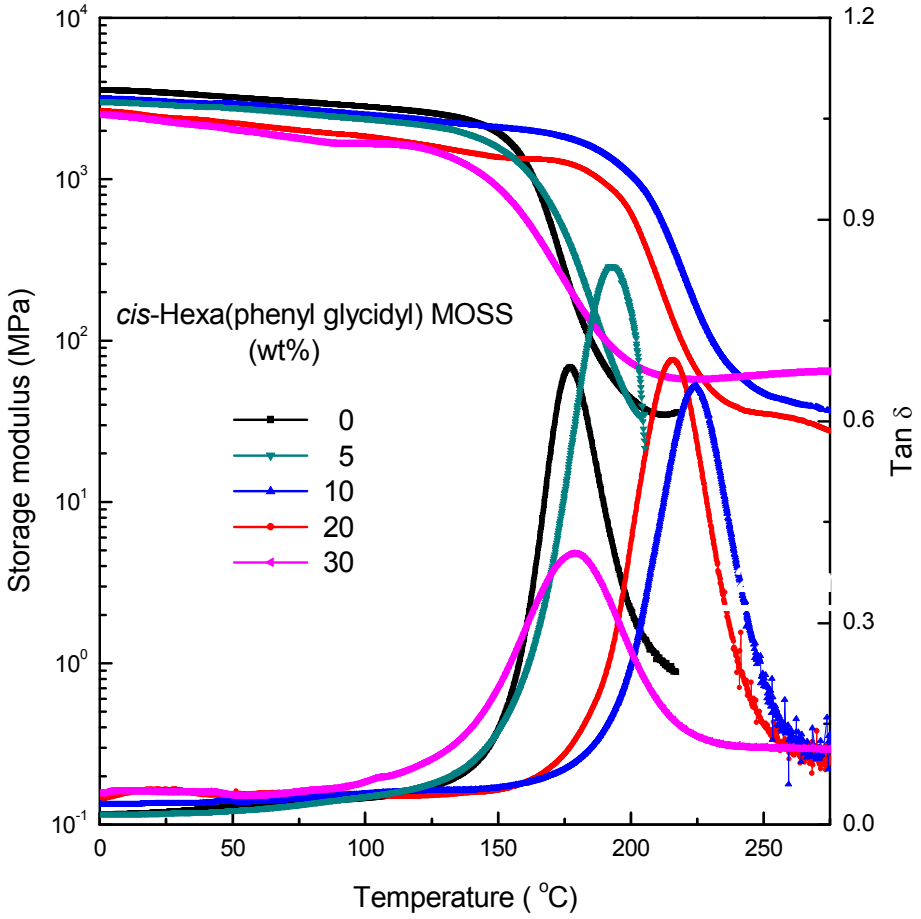
Storage modulus (MPa)
Tan δ
Temperature (°C)
cis-Hexa(phenyl glycidyl) MOSS
(wt%)
0
5
10
20
30

Figure 11

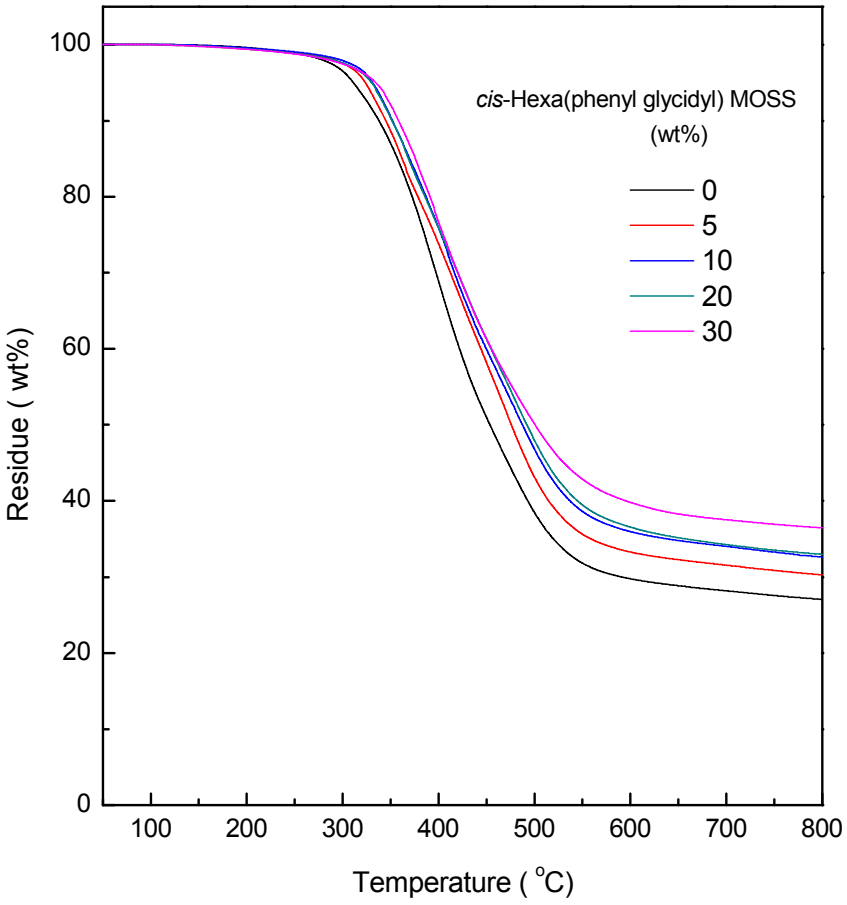
100
80
60
40
20
0
Residue (wt%)
100
200
300
400
500
600
700
800
Temperature (°C)
cis-Hexa(phenyl glycidyl) MOSS
(wt%)
0
5
10
20
30

Figure 12

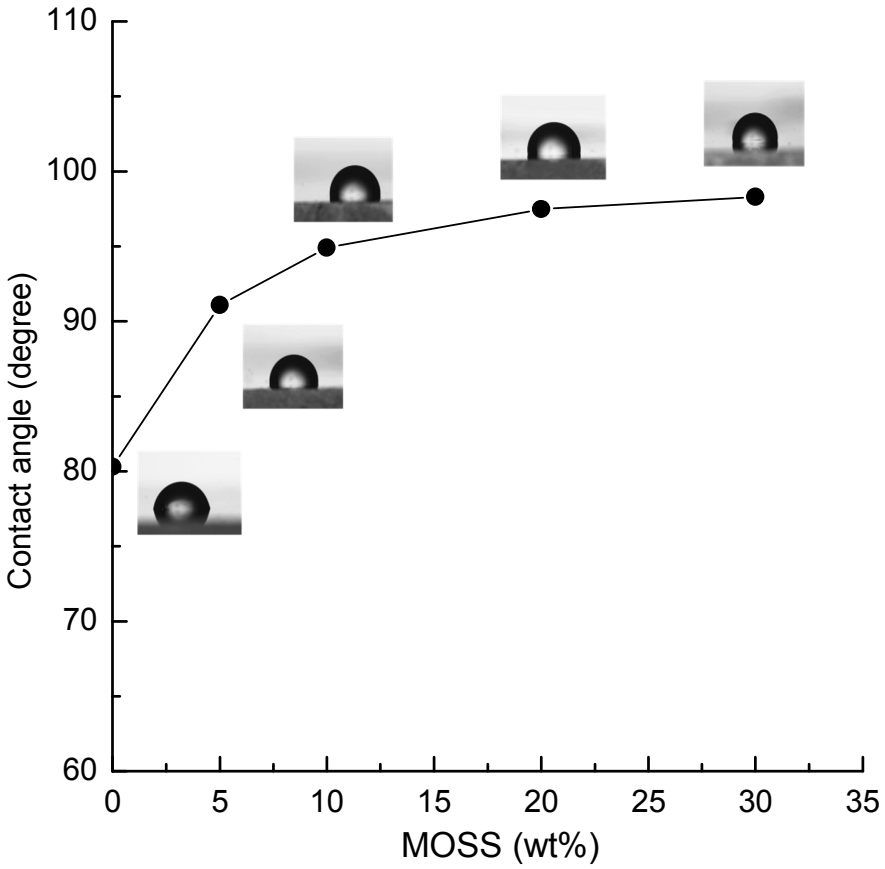
110
100
90
80
70
60
Contact angle (degree)
0
5
10
15
20
25
30
35
MOSS (wt%)

Figure 13